ACS OMEGA

http://pubs.acs.org/journal/acsodf

Article

Stable Encapsulation of Methylene Blue in Polysulfide Organosilica Colloids for Fluorescent Tracking of Nanoparticle Uptake in Cells

Guann-Tyng Chen and Teh-Min Hu*

Cite This: *ACS Omega* 2021, 6, 32109−32119

Read Online

ACCESS | Metrics & More | Article Recommendations

ABSTRACT: Methylene blue (MB), a century-old drug and a fluorescent dye, has a long history of diverse applications, both in drug therapy and as a tissue-staining agent. However, MB is inherently unstable when exposed to light and reducing agents. In this study, we aim to prepare and characterize polysulfide-based organosilica colloidal particles for efficient, stable, and protective encapsulation of MB. Disulfide- and tetrasulfide-containing organosilane congeners were used as organosilica precursors for direct synthesis of organosilica colloids based on the silica ouzo effect. MB was spontaneously entrapped into the colloidal particles during the particle formation process. The following properties of the colloidal MB were evaluated: particle size, surface charge, atomic distribution, encapsulation efficiency, MB release, photodynamic activity, thiol and ascorbate reactivity, and cytotoxicity. The DLS measurements show that the size of colloidal MB is tunable in a range of 100 nm to 1 μm. SEM images reveal spherical particles with composition-dependent particle sizes of 70−120 nm (coefficient of variation: 15−18%). MB was encapsulated in the colloidal particles with a maximal efficiency of 95%. The release of MB from the colloids was <1% at 4 h and <3.5% at 48 h. The colloidal particles show much reduced photodynamic activity, low reactivity toward reducing agents, and low cytotoxicity. Accordingly, the colloidal MB was proposed and further investigated as a fluorescent particle tracer for the study of cell−nanoparticle interactions. In conclusion, MB can be efficiently and stably loaded into polysulfide organosilica colloidal particles using a simple and convenient physical route.

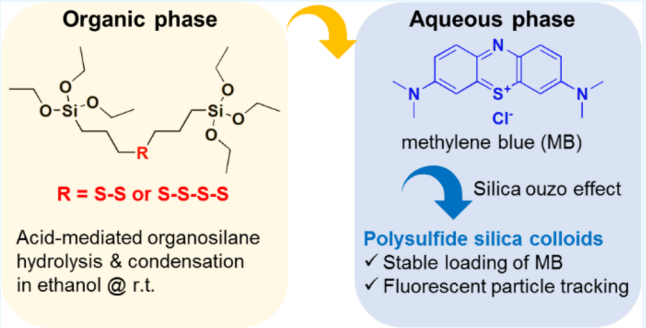

1. INTRODUCTION

Methylene blue (MB) has been used as a drug for over 130 years.[1] MB was first synthesized in 1876 as an aniline-based dye for the textile industry.[2] In 1891, it was used in the treatment of malaria.[1] Nowadays, MB is still used in clinical situations, including treatment of methemoglobinemia[3] and as a tissue-staining dye during surgery.[4] The drug has also been proposed in the treatment of septic shock,[5] ifosfamide-induced encephalopathy,[6,7] Alzheimer's disorder,[8] and even COVID-19.[9] Currently, several clinical trials are registered in ClinicalTrials.gov for various treatments, including septic shock, diabetic lower limb ulcer, deep tissue abscess, halitosis, and COVID-19.

MB has been investigated as a photosensitizer in photodynamic therapy owing to the photosensitive property of its phenothiazine structure.[10−12] However, the in vivo photodynamic activity of MB was limited by its inherent instability in the physiologically reducing milieu and by nonspecific tissue distribution. To increase the photodynamic activity of MB, various nanoparticle-based carriers have been extensively investigated. The materials used for preparing the nanocarriers include lipid,[13] silica,[14−17] protein,[18] organic polymers,[19−21] graphene oxide,[22,23] and gold.[24−26] Although nanocarriers improved photodynamic activity, the stability and release of MB in nanocarriers have not been fully addressed in previous studies.

In the last decade, thiol-responsive nanodrug delivery systems have been extensively studied based on the rationale of high intracellular glutathione (GSH) concentrations.[27] GSH-responsiveness was engineered into nanocarriers by the incorporation of disulfide linkages within the carrier matrix.[27,28] The disulfide bonds are expected, and have been shown, to be breakable in the presence of thiols through the thiol-disulfide exchange reaction.[29,30] Accordingly, the literature is awash with reports of thiol-responsive drug nanocarriers. Sulfide-functionalized silane precursors have been frequently used to prepare polysulfide silica nanoparticles through a sol−gel condensation reaction.[28,31−33] The concept

Received: September 4, 2021
Accepted: November 2, 2021
Published: November 16, 2021

Scheme 1. Schematic Illustration of the Proposed Method for Preparation of Methylene Blue-Loaded Colloidal Particles from Disulfide and/or Tetrasulfide Organosilane Congeners

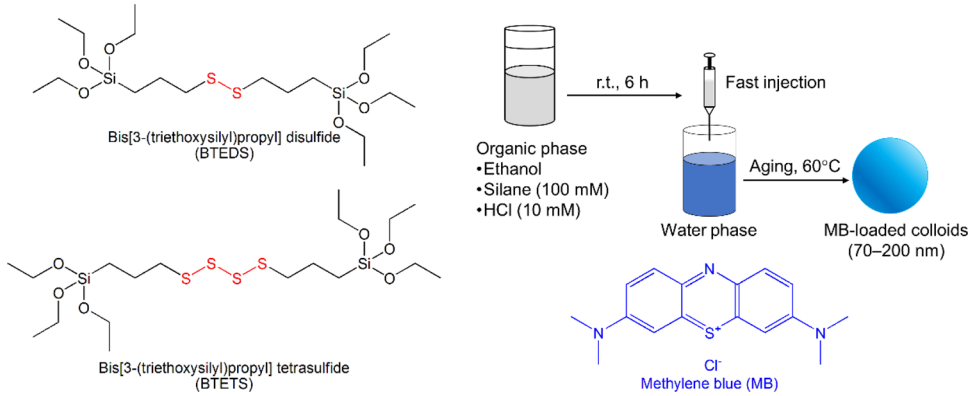

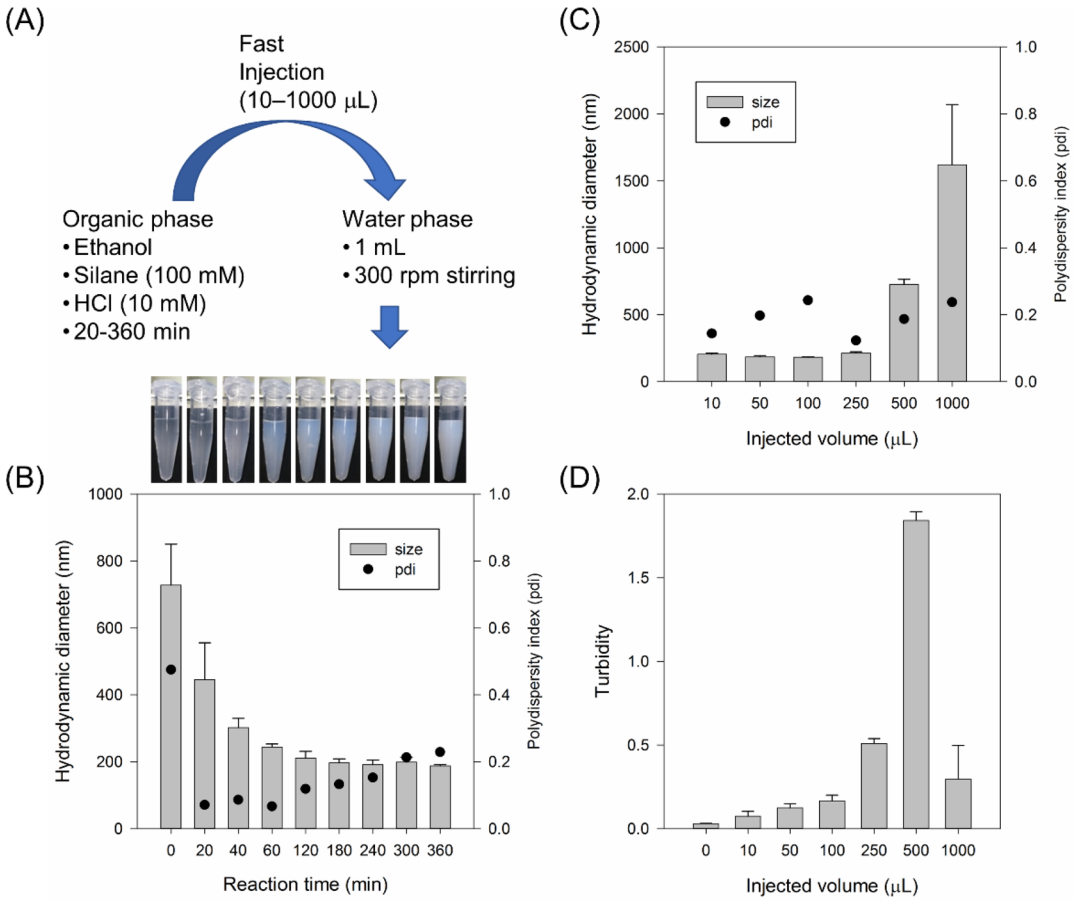

Figure 1. Preparation of polysulfide organosilica colloids based on the silica ouzo effect. (A) Schematic of the basic step and compositions. Sulfide-containing organosilanes (100 mM) were dissolved in ethanol to make an organic phase. After 20−360 min of reaction under the catalysis by 10 mM of HCl, an aliquot of the organic phase was taken and injected to 1 mL of water. (B) Effect of organic-phase reaction time on particle formation. (C) Effect of the volume of organic phase injected on particle formation (size and size distribution). (D) Turbidity of the final solution formed as a function of injected volume. At an injected volume of 1 mL, rapid sedimentation of large particles resulted in underestimated turbidity with high variability.

has been demonstrated in many studies, using mostly doxorubicin as a model drug.[34−39] Other loading includes pyrene,[40] cytochrome c,[41] and RNase.[42] The properties of polysulfide silica nanoparticles vary with the use of different silane precursors and methods and/or conditions used to prepare them. In fact, thiol responsiveness is not straightforward, which is highly dependent on the particle structure and properties, including degree of silica condensation, sulfide contents, pore sizes, shell thickness, and surface modifications.[30]

In this study, we propose a method to prepare MB-loaded polysulfide organosilica colloids. To the best of our knowledge, MB has not been loaded into similar colloidal systems. Our approach uses disulfide and tetrasulfide organosilane precursors (Scheme 1) as the building blocks of polysulfide organosilica. The formation of colloidal particles was mediated

https://doi.org/10.1021/acsomega.1c04877
ACS Omega 2021, 6, 32109−32119

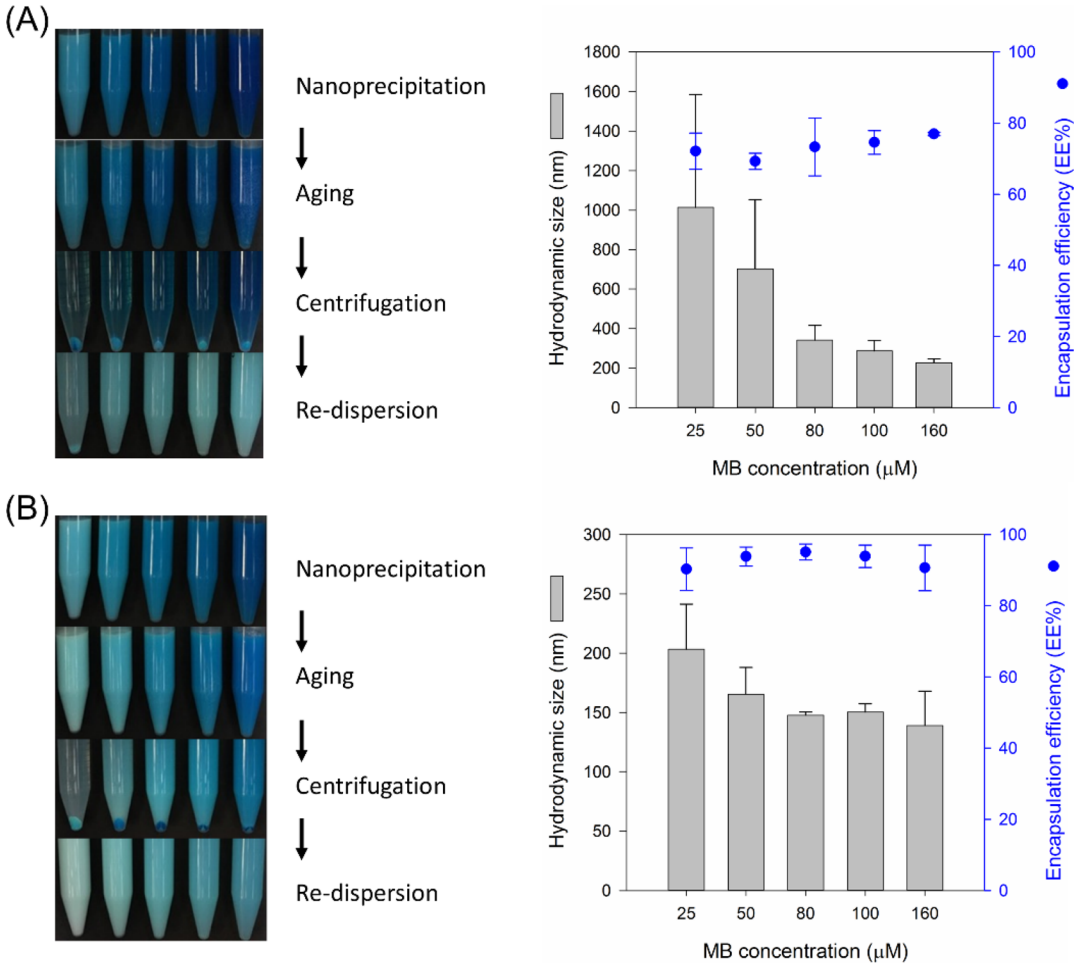

Figure 2. Preparation of colloidal MB from (A) disulfide organosilane precursor and (B) tetrasulfide organosilane precursor. The photographic images were those of the final solutions at different stages after injecting the organic phase into the MB-containing water phase; from left to right, MB concentrations in the water phase are 25, 50, 80, 100, and 160 μM. The resulting colloidal solutions show MB-concentration dependent particle size and encapsulation efficiency (mean ± S.D.; n = 3).

by a so-called silica ouzo effect, which was previously described by our group for other silane precursors.[43,44] Our polysulfide organosilica colloids show high and stable encapsulation of MB with limited release, high shielding effect against reducing substances, and low thiol reactivity as well as low cytotoxicity. With such properties, the colloidal MB preparation was proposed as a fluorescent particle tracer for studying cellular uptake kinetics of colloidal particles.

2. RESULTS AND DISCUSSION

2.1. Colloid Formation Based on the "Silica Ouzo Effect". Previously, polysulfide-containing organosilica particles have been prepared from traditional base-catalyzed reaction involving co-condensation of a disulfide- or tetrasulfide-functionalized organosilane with a tetraalkyl orthosilicate.[45] In this study, we introduced a different approach to prepare polysulfide organosilica particles using only disulfide- and/or tetrasulfide-organosilanes as the silica source. The method is a modification of our previous work on the so-called silica ouzo effect.[46−49] Figure 1 shows the schematic procedure of the preparation and the results of parameter optimization. The preparation involved an organic phase in which the organosilane was dissolved and condensed in an acidic environment. After several runs of testing, the organic phase parameters were optimized for silane concentrations, the choice of solvent, and acidity of the reaction. The best solvent was determined to be 95% ethanol in which disulfide-organosilane (BTEDS) was dissolved. BTEDS underwent hydrolysis and silica condensation in the presence of 10 mM HCl. The reaction time is an important parameter because it determines the degree of organosilica condensation that forms water-insoluble condensed species. The optimal reaction time was determined by visual evidence of colloid formation and by particle size measurements, which were conducted immediately after injecting the organic phase to the water phase. As can be seen, milky white colloids were visibly evident at a reaction time of ≥60 min (see inserted photo images). Moreover, the particles that formed after 180−360 min of reaction have hydrodynamic sizes of around 200 nm with a polydispersity index of <0.2 (Figure 1B). Since a 6 h reaction produced particles that were more abundant, stable, and easier to collect, the reaction time was fixed at 6 h in the following experiments. Figure 1C shows that particle sizes increased with the injected volume of the organic phase, and the optimal volume was determined to be 0.25 mL (injected to the 1 mL water phase) based on the particle size distribution (polydispersity data) and relative abundance of particles formed (i.e., turbidity comparison between conditions that produced particles with similar sizes, Figure 1D).

https://doi.org/10.1021/acsomega.1c04877
ACS Omega 2021, 6, 32109−32119

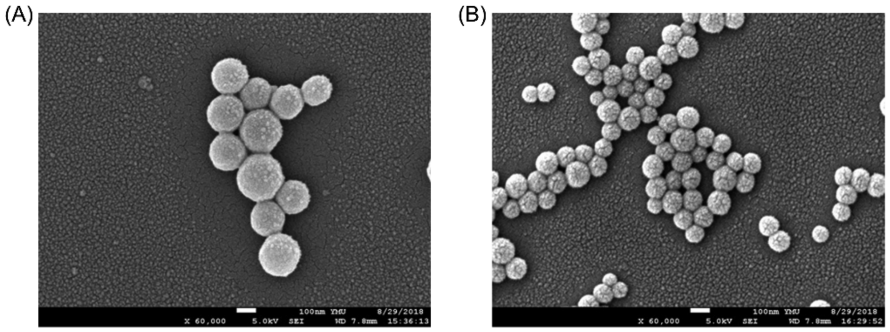

	Wt%	amu	Wt%/amu	Atomic %
O	52.3	16	3.27	59.5
Si	33.9	28.09	1.21	22.0
C	10.3	12.01	0.86	15.6
S	2.2	32.07	0.07	1.2
N	1.3	14	0.09	1.7

	Wt%	amu	Wt/amu	Atomic %
O	47.3	16	2.96	52.9
Si	28.5	28.09	1.01	18.1
C	15.5	12.01	1.29	23.1
S	7.8	32.07	0.24	4.4
N	1.2	14	0.09	1.5

Figure 3. Particle morphology (SEM images) and chemical composition (from EDS analysis) of polysulfide organosilica colloidal particles. (A) Preparation from the disulfide precursor (i.e., BTEDS) alone. (B) Preparation from the tetrasulfide precursor (i.e., BTETS) alone.

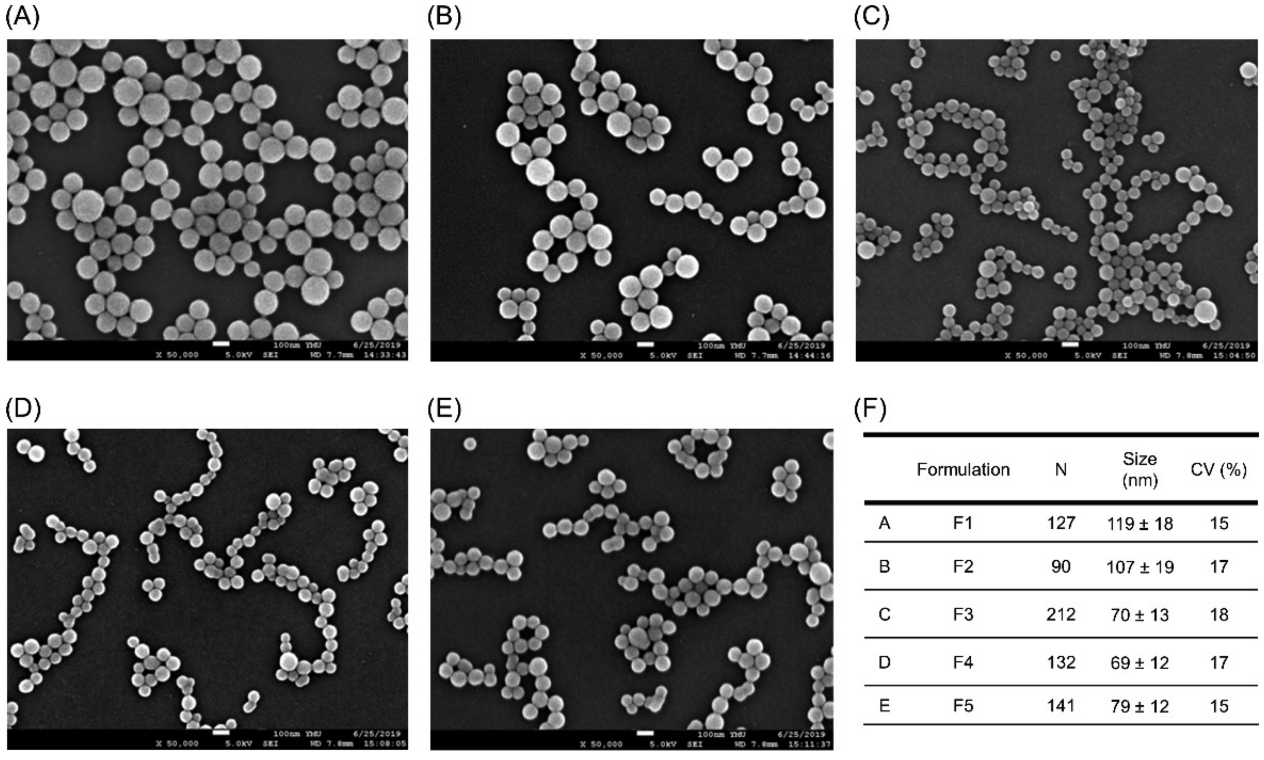

	Formulation	N	Size (nm)	CV (%)
A	F1	127	119 ± 18	15
B	F2	90	107 ± 19	17
C	F3	212	70 ± 13	18
D	F4	132	69 ± 12	17
E	F5	141	79 ± 12	15

Figure 4. Morphology and size of particles obtained from various formulations. Colloidal particles were prepared with different compositions of silane precursors: (A) BTEDS alone, (B) 80% BTEDS + 20% BTETS, (C) 50% BTEDS + 50% BTETS, (D) 20% BTEDS + 80% BTETS, and (E) BTETS alone. (F) Particle size analyzed by ImageJ. *N* = number of particles analyzed. The white scale bar in each image represents 100 nm.

2.2. Encapsulation of Methylene Blue (MB). Disulfide-silane (BTEDS) and tetrasulfide-silane (BTETS) were included as polysulfide-organosilica precursors to investigate the preparation conditions for the encapsulation of methylene blue. First, BTEDS was used as a single precursor for encapsulation of MB at various concentrations. Blue colloids were formed at all MB concentrations (Figure 2A). Under a high-speed (6000*g*) centrifugation protocol, particle pellets were visible in the bottom of the tube. After removing the supernatant, water was added to the pellet followed by vigorous pipetting (i.e., up and down for 30 s with a P1000 pipette). The photo images of Figure 2A show that most particles were redispersible, leaving no residual pellet after pipetting. However, the particle prepared at a low MB concentration (i.e., 25 μM) was only slightly redispersible with a visible pellet trace. This observation is consistent with

https://doi.org/10.1021/acsomega.1c04877
ACS Omega 2021, 6, 32109−32119

the result of particle size measurements for the redispersed particles: larger particles were measured for particles prepared at lower MB concentrations (Figure 2A). The data suggest that the particles prepared at a low [MB] were less stable and more prone to aggregate. More stable colloidal particles (size: <0.5 μm) were produced at [MB] $\geq$ 80 μM (Figure 2A). Taken together, MB seems to play a role in facilitating the formation of a colloidal structure. For particles prepared with the disulfide silane, the encapsulation efficiency of MB was greater than 60% at all MB concentrations (Figure 2A).

Second, the tetrasulfide-silane (BTETS) was tested under the same preparation conditions. As can be seen, particles produced were redispersible for all MB concentrations (photo images, Figure 2B). In addition, after washing, particles with hydrodynamic sizes of <200 nm were collectable (data, Figure 2B) and the encapsulation efficiency can be as high as 90% (Figure 2B). The results suggest that the tetrasulfide silane precursor has a higher tendency than the disulfide counterpart in forming a self-assembled structure after condensation. This conjecture is consistent with the SEM images showing much smaller particles for the tetrasulfide than disulfide samples (Figure 3). The atomic distribution of the particle was revealed by EDS measurements applied to the SEM sample. A higher percentage of sulfur was detected in the sample prepared from the tetrasulfide silane.

To demonstrate the versatility of the proposed method, the two silanes at various proportions were used to form mixed silane precursors in the preparation. As shown in Figure 4, the colloidal particles were almost homogeneous under the microscopic field of SEM (images A–E). The mean particle sizes decrease with increasing fractions of tetrasulfide component, from ~120 nm down to ~70 nm (Figure 4F). The coefficient of variation (%CV) is less than 20%. Moreover, the encapsulation efficiency was tunable from ~60 to 80% (Figure 5). The mixed-sulfide particle preparations showed comparable hydrodynamic size distributions in water and in a culture medium (Figure 6A). The particles were negatively charged (−20 mV) in pure water. In the culture medium with serum, the negativity of the surface charge was significantly reduced to a nearly neutral value (Figure 6B), suggesting coverage of proteins on the particle surface.

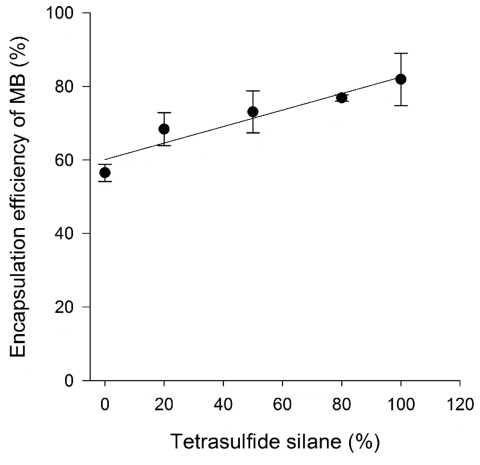

Figure 5. Encapsulation efficiency of MB in colloidal MB formulations with varied composition of disulfide and tetrasulfide silane precursors. An aliquot of 0.2 mL of the organic phase (containing BTEDS and/or BTETS at various ratios, after 6 h of reaction) was injected into 0.8 mL of water containing 160 μM MB. After centrifugation (21,130*g*, 25 °C, 15 min), the remaining concentration of MB in the supernatant was determined for the estimation of encapsulation efficiency. Mean ± S.D. (n = 3).

2.3. Release and Photodynamic Activity of MB-Loaded Colloids. A dialysis-bag approach was used to determine the rate and extent of MB released from particles. Figure 7 indicates that, compared with fast and complete release of free MB (control), release of MB from MB-colloid was almost undetectable within 10 h; the maximum release was about 3% at 48 h. The result indicates that MB is very stably incorporated in the particle matrix.

The photodynamic activity of MB-loaded colloids was tested with a method modified from He et al.[15] Under red-light irradiation, the fluorescence intensity of a fluorescent chemical probe, 1,3-diphenyl-2-benzofuran (DPBF), was reduced by the presence of MB. Figure 8 shows a first-order kinetic decay of the fluorescence intensity. The data show that free MB exerted a fast fluorescent quenching effect with an estimated first-order rate constant of 0.012 s^{-1}. However, all colloidal formulations (F1–F5), regardless of silane composition, show markedly diminished photodynamic activity (~25% of free MB). The result reinforces that MB is firmly and stably sequestered in the particle matrix, thereby limiting the direct interaction of MB-derived reactive species with the fluorescent probe.

2.4. Reactivity toward Reducing Agents. Polysulfide-containing silica particles have been considered as thiol-responsive, which is a promising property for biomaterials of various applications.[27,28] The rationale is that disulfide or polysulfide linkages would react with high abundance of endogenous thiols such as glutathione (GSH) or cysteine.[29,30] The resulting breakage of the sulfide linkage is expected to cause disassembly of the particle structure, thereby allowing the payload to be released in a thiol-responsive manner. To test the thiol reactivity of our polysulfide colloids, we first incubated colloids with glutathione and measured the concentrations of GSH over time. The results show that the decay rate of GSH levels in solution increases with increasing particle concentrations (Figure 9). However, the reaction is slow (i.e., 6–11% per hour, based on the magnitude of the first-order rate constant). We further investigated whether incubation of polysulfide particles with a high concentration (10 mM) of GSH or DTT (dithiothreitol) would affect the particle size. The result shows that particle sizes did not change significantly over 120 h of incubation (data not shown). The finding is consistent with a low surface sulfur content observed from the EDS analysis (Figure 3). Low accessibility of disulfide bonds may account for high stability of our particles.

MB is known to rapidly react with ascorbic acid, resulting in loss of its blue color (bleaching).[50] Conceivably, if MB was stably packed in a colloidal matrix, then the ascorbate-mediated bleaching effect would be prevented because of limited MB accessibility. Figure 10 demonstrates the protective effect of the colloidal particle against ascorbate-mediated bleaching of MB. It shows that free MB solution lost its blue color even at the lowest concentration (i.e., 10 mM) of ascorbate (Figure 10B). In comparison, MB-colloids remained blue at the highest concentrations (100 mM) of ascorbate (Figure 10A). After centrifugation, the blue particle pellets were clearly visible at the bottom of tubes.

2.5. Cytotoxicity. The cytotoxicity of MB-loaded colloids was investigated using the MTT assay. While free MB showed slight cytotoxicity against some cell lines, the MB-loaded

https://doi.org/10.1021/acsomega.1c04877
ACS Omega 2021, 6, 32109−32119

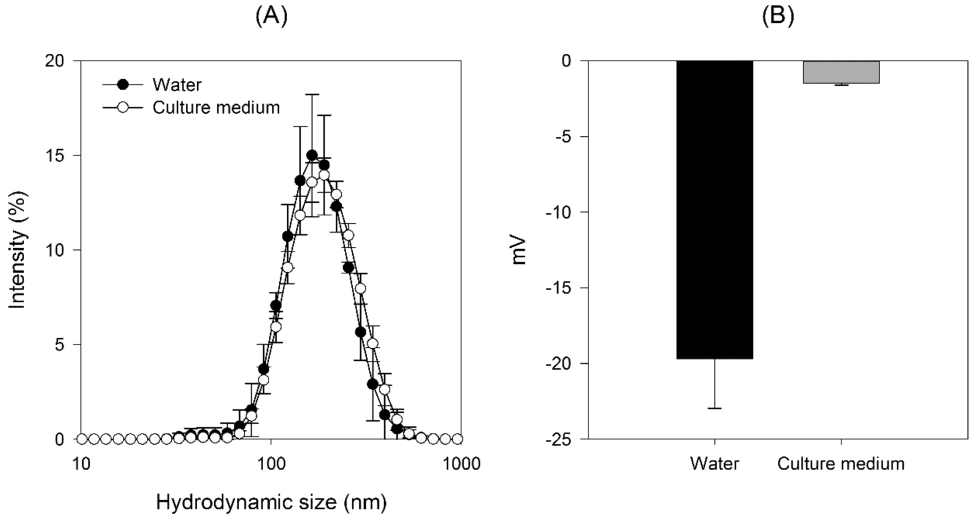

Figure 6. (A) Hydrodynamic particle size distribution and (B) zeta potential of colloidal MB in water and culture medium. Colloidal MB was prepared from mixed silane (50% BTEDS and 50% BTETS). Mean ± S.D. (n = 3).

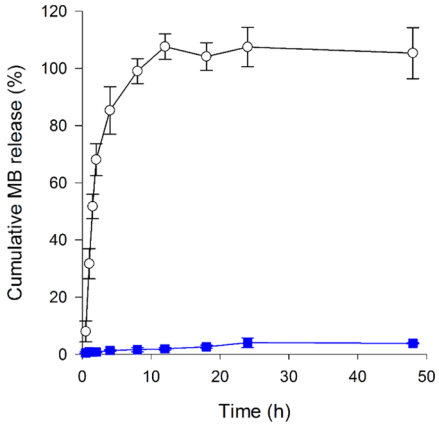

Figure 7. Release profile of colloidal MB compared with that of free MB. A 1 mL solution of colloidal MB (prepared from mixed silane of BTEDS and BTETS at a 1:1 ratio) or free MB at an equivalent concentration of 50 μM was added into a dialysis bag (1 mL), which was then immersed in 250 mL of PBS followed by the procedures described in Section 4. Mean ± S.D. (n = 3).

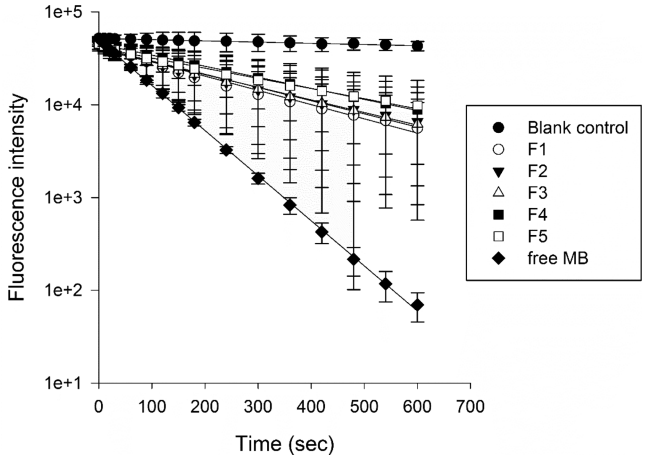

Figure 8. Photodynamic activity of colloidal MB compared with that of free MB. Five formulations (F1−F5, as described in Figure 4) of colloidal MB and free MB were tested at an MB concentration of 5 μM. The reaction solution contains 10 μM 1,3-diphenyl-2-benzofuran (DPBF, as the chemical probe) in ethanol. Blank control: ethanol. Mean ± S.D. (n = 3).

colloid showed much reduced cytotoxicity or no toxicity at the tested concentration range (Figure 11).

2.6. Cellular Uptake. The polysulfide organosilica colloids represent a new class of nanocarriers for MB. Our MB-colloids have the following features: high and stable MB-loading and low cytotoxicity. Such properties may have little therapeutic potential owing to limited MB release. However, the low-release potential of fluorescent MB is ideal for tracing particles during cellular transport of colloidal particles. To demonstrate this premise, we conducted a preliminary cellular uptake study using both direct fluorescent measurements and flow cytometry. As expected, the direct measurement showed substantial cellular MB uptake after incubating a cancer cell line with free MB (Figure 12); the percent uptake reached 37% after 4 h of incubation. In contrast, the cellular uptake of the MB-colloid was only 0.7%, indicating very low cellular uptake of nanoparticles.[51] The flow cytometric data shown in Figure 13 are consistent with the direct fluorometric assays.

3. CONCLUSIONS

In this study, MB was encapsulated in polysulfide organosilica colloids with high efficiency and stability. We demonstrate that colloidal particles can be directly formed from disulfide and/or tetrasulfide organosilanes based on the silica ouzo effect. The proposed method allows for preparing colloidal MB with tunable particle size (70−120 nm) and loading (encapsulation efficiency 60−80%). MB was stably entrapped within the organosilica matrix, with low MB release (<1% at 4 h and <3.5% at 48 h), low reactivity toward light and reducing agents, and low cytotoxicity. Having the abovementioned properties, we envision a new application of colloidal MB as a fluorescent particle tracer for the study of nano-bio-interactions.

4. MATERIALS AND METHODS

4.1. Chemicals. Bis[3-(triethoxysilyl)propyl] disulfide (BTEDS) and bis[3-(triethoxysilyl)propyl] tetrasulfide (BTETS) were obtained from Gelest (USA). Dimethyl

https://doi.org/10.1021/acsomega.1c04877
ACS Omega 2021, 6, 32109−32119

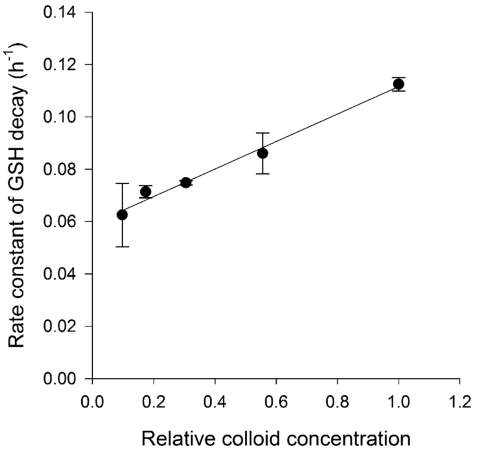

Figure 9. GSH decomposition rate as a function of relative concentration of polysulfide colloid. The first-order rate constant was determined from the log-linear kinetic profile of GSH disappearance over 12 h in the presence of various colloid concentrations. Colloidal MB was prepared with BTEDS/BTETS at a 1:1 ratio. After purification, colloidal particles were redispersed in water and the turbidity of the colloidal dispersion was measured. Serial dilutions were performed to prepare samples with different colloidal concentrations (relative to an initial concentration). Mean ± S.D. (n = 3).

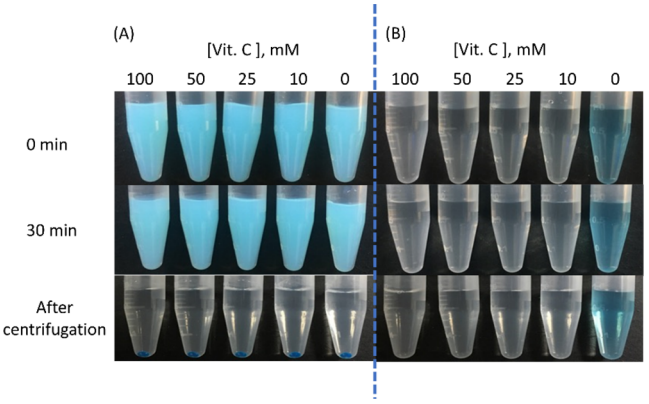

Figure 10. Ascorbate reactivity. (A) Colloidal MB. (B) Free MB. Colloidal MB and free MB (10 μM) were mixed with an equal volume of ascorbate solution. Blue-colored particles were recovered as blue pellets after centrifugation in the colloidal MB group.

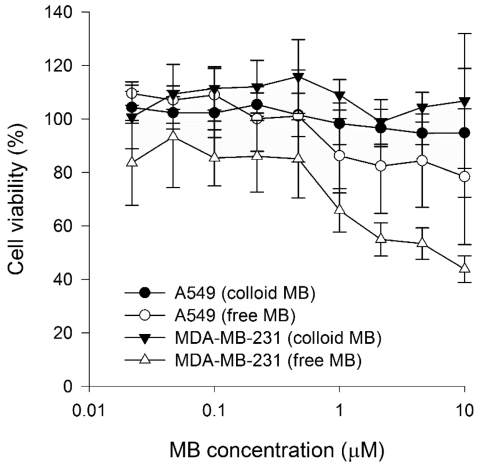

Figure 11. Cytotoxicity of colloidal MB and free MB. Cell viability (after 24 h of treatment) was measured using the MTT assay. Data are expressed as % of control treatment (without MB); mean ± S.D. (n = 3).

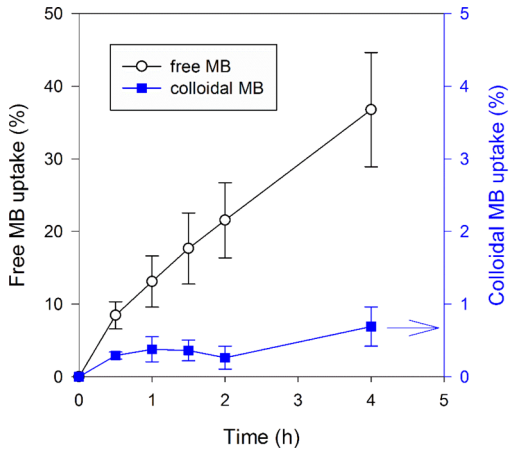

Figure 12. Cellular uptake of colloidal MB and free MB determined by a direct fluorometric assay. A549 cells treated with colloidal MB or free MB (6.25 μM) in PBS. The amount of intracellular MB was extracted and directly determined based on a fluorometric standard curve of MB. Data are expressed as % uptake (relative to the total amount of MB added); mean ± S.D. (n = 3).

sulfoxide and Tris base were from J.T. Baker (USA). The following materials were from Sigma-Aldrich (USA): methylene blue hydrate, poly(vinyl alcohol) (PVA, MW: 9000–10,000, 80% hydrolyzed), glutathione reduced, paraformaldehyde, DMEM, powder, 5,5′-dithiobis(2-nitrobenzoic acid, DTNB), and sodium acetate. An F-12K medium was obtained from Corning (USA). Ethanol (>99%) was from Honeywell (Germany). Hydrochloric acid was from Merck (Germany). Fetal bovine serum, penicillin, and streptomycin were purchased from Gibco (USA). Deionized water (18.2 MΩ·cm at 25 °C) was used throughout the study (ELGA Ultra Scientific water-purification system, France).

4.2. General Procedures of the Silica Ouzo Effect. In this study, the preparation of this MB-loaded polysulfide colloid was modified from our previous study.[46−49] The organosilanes used were organosilanes with disulfide and tetrasulfide linkages (Scheme 1). The silica ouzo effect involves solvent shifting between an organic (solvent) phase and a water (non-solvent) phase. Ethanol was used throughout as the main solvent. Briefly, the organosilane precursor (0.514−0.547 mL of the original solution, depending on silane composition) was first dissolved in ethanol (8.95−8.98 mL) followed by adding HCl (0.5 mL, 200 mM) to make an alcoholic solution containing 100 mM silane and 10 mM HCl in a total volume of 10 mL. The organic phase was placed in the dark without stirring at room temperature. At the end of a predetermined reaction time, an aliquot of the organic phase was taken and rapidly injected into deionized water. For small volume preparation, a micropipette was used to withdraw and inject the organic phase (e.g., 0.25 mL, unless otherwise specified) into a 1 mL water phase in microcentrifuge tubes. For a larger scale, a syringe with a 27G needle was used to take and inject (within 4 s) an aliquot of the organic phase (e.g., 2.5 mL) into the 10 mL water phase (with constant stirring at 300 rpm). For drug loading, the water phase was made to contain methylene blue at 160 μM (unless otherwise specified) before the solvent-shifting process.

https://doi.org/10.1021/acsomega.1c04877
ACS Omega 2021, 6, 32109−32119

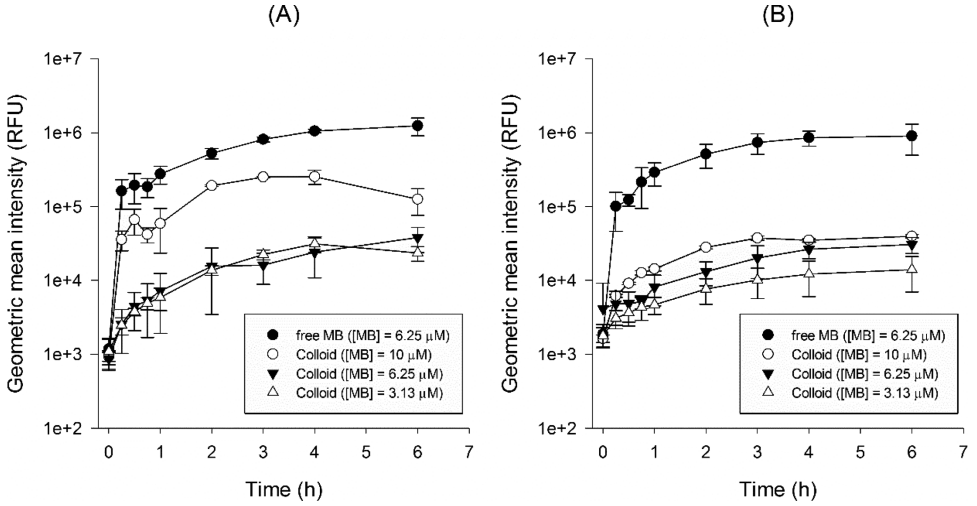

Figure 13. Kinetics of cellular uptake of colloidal MB and free MB determined by flow cytometry. (A) A549 cells. (B) MDA-MB 231 cells. Mean ± S.D. (n = 3).

4.3. Preparation of MB-Loaded Polysulfide. To find the optimal MB concentrations, the water phase was added with various concentrations of MB (25−160 μM). The organic phase contained either the disulfide silane or the tetrasulfide silane (100 mM) dissolved in ethanol with 10 mM HCl. The organic phase was then allowed to stand at room temperature in the dark for 6 h followed by rapidly injecting 2.5 mL of the organic phase to 10 mL of the water phase. The resulting colloidal solution was kept at 60 °C for 1 h (aging) followed by adding with an equal volume of 0.2% PVA aqueous solution. Then, the colloidal particles were purified and collected by extensive centrifugation and replacement of fresh water three times. Finally, the particle pellets were resuspended with water and subjected to measurements of particle sizes and encapsulation efficiency.

The effect of varying silane composition on particle formation and MB encapsulation was further investigated. The concentration of MB in the water phase was fixed at 160 μM. The composition of the organic phase was modified to contain a mixture of the two polysulfide silica precursors, BTEDS and BTETS, at different combination ratios, i.e., 100% BTEDS, BTEDS/BTEDS = 80%/20%, 50%/50%; 20%/80%, and 100% BTETS. All the other conditions, including solvent shifting, aging, and washing, were kept unchanged, unless otherwise specified.

Hydrodynamic diameters and zeta potentials were recorded based on dynamic light scattering (Zetasizer Nano, Malvern, UK). The encapsulation efficiency (EE%) of MB was estimated from the fluorescence measurement (excitation/emission = 610 nm/690 nm, gain = 117; Spark 10M, TECAN, Austria) of remaining MB in the supernatant using the following equation: EE (%) = $(C_{\text{theoretical}} - C_{\text{supernatant}})/C_{\text{theoretical}} \times 100$, where $C_{\text{theoretical}}$ represents the theoretical concentration of MB in the final solution without particles and $C_{\text{supernatant}}$ is the concentration of MB in the supernatant after nanoprecipitation.

4.4. Scanning Electron Microscopic (SEM) Analysis. The morphology of the colloidal particles was examined by a field-emission scanning electron microscope (JEOL, JSM-7600F). The colloid sample (1 μL) was placed on a glass cover slip and then air-dried overnight. After platinum coating for 120 s using metal deposition (vacuum evaporator, JEE-400; auto fine coater, JFC-1600), the image was taken at 5.0 kV, SEI mode. The SEM samples were further evaluated for the atomic distribution using energy dispersive X-ray analysis (EDS; Oxford Aztec X-Max80).

4.5. Release of MB from Colloidal Particles. A 1 mL sample (free MB solution or MB-loaded colloids) was added in a dialysis bag (molecular cutoff = 12−14 kD). The concentration of MB in the initially added sample was 50 μM. The bag was immersed in 250 mL of PBS (pH 7.4, 37 °C) under constant stirring (300 rpm). After each sampling time, 25 mL of the release medium was taken for assay and the original solution supplemented with the same volume of fresh PBS. The concentration of MB was directly measured using a fluorescent microplate reader (excitation/emission = 610 nm/690 nm, gain = 117; Spark 10M, TECAN, Austria). The cumulative amount of MB release (expressed as percentage of initially added amount) was estimated using the following equation: $\%\text{release} = 100 \times (V_s\sum_i^{n-1} C_i + V_0C_n)/A$, where V_s is the sampling volume (25 mL); V_0 is the total volume of the release medium, i.e., 250 mL; C_i is the concentration of analyte at each time point (i = 1 to n); and A is the total drug amount initially added.

4.6. Photodynamic Activity. The method reported by He et al.[15] was used with modification. The MB-loaded colloidal preparations (containing 10 μM MB) was centrifuged at 9000g (25 °C, 15 min) followed by removal of the supernatant. The particle pellet was redispersed in equal volume of ethanol. 1,3-Diphenylisobenzofuran (DPBF) was used as a fluorescent indicator. The indicator solution was freshly prepared and diluted in ethanol to make a final concentration of 20 μM DPBF (avoiding light during and after preparation). An aliquot of 50 μL ethanolic particle solution was then mixed with an equal volume of the indicator solution to start the kinetic measurements (0−600 s) under the irradiation of red LED light (at 640 nm, 2400 lux). The fluorescence intensity was recorded at an excitation/emission of 384 nm/450 nm (gain = 60).

4.7. Reactivity of Polysulfide Colloidal Particles toward Reducing Agents. Glutathione (GSH) was dissolved and diluted in a 100 mM phosphate buffer to make a 200 μM GSH solution. MB-loaded colloidal particles (prepared from mixed silanes of BTEDS/BTETS = 50%/50%)

https://doi.org/10.1021/acsomega.1c04877
ACS Omega 2021, 6, 32109−32119

were dispersed in 1 mL of the phosphate buffer followed by twofold serial dilutions to prepare five samples with different particle concentrations. Then, 1 mL of each sample was mixed with 1 mL of GSH solution. The final solution mixtures have turbidity (absorbance at λ = 800 nm) readings of 1.48, 0.80, 0.44, 0.25, and 0.14. At each sampling time, 0.2 mL of the solution mixture was taken for centrifugation (21,130*g*, 15 min). The supernatant (100 μL) was mixed with the same volume of Ellman's reagent (containing DTNB (0.2 mM), sodium acetate (5 mM), and Tris base (200 mM)) for 15 min to determine the remaining GSH concentration.

To test the reactivity with ascorbate, 0.5 mL of free MB or a particle preparation (containing 10 μM MB) was directly mixed with 0.5 mL of ascorbate solutions (with final concentrations after mixing ranging from 10 to 100 mM). The mixtures were then observed at room temperature for 30 min.

4.8. Cell Culture and Cytotoxicity Assay. A549 and MDA-MB-231 were purchased from Bioresource Collection and Research Center (BCRC) in Taiwan. A549 was cultured in Ham's F-12K (Kaighn's) medium. MDA-MB-231 was cultured in Dulbecco's modified Eagle medium. All culture media were supplemented with 10% fetal bovine serum, 100 IU/mL penicillin, and 100 μg/mL streptomycin. Cells were incubated in a humidified controlled atmosphere with an air/CO_2 ratio of 95%/5% at 37 °C.

Cytotoxicity of free MB and colloidal was determined by the MTT assay. All cell lines were seeded and incubated in 96-well plates (3599, Costar) at a density of 2×10^4 cells/well. After 24 h, the culture medium in each well was removed and then replaced with a medium containing free MB or colloidal MB at various concentrations (up to 100 μM). After 24 h of incubation, the drug-containing medium was removed, and to each well 100 μL of MTT (0.5 mg/mL) was added and incubated for 3 h. After removing the MTT solution, DMSO (100 μL/well) was added to dissolve the formazan dye. The absorbance at 570 nm was measured using a microplate reader (Spark 10M, TECAN, Austria). The cell viability was expressed as percentage of measured absorbance of MB-treated wells relative to that of the medium-control well. Data were obtained from three independent experiments.

4.9. Cell Uptake Kinetics. The direct fluorometric method was used with modification.[52] For the direct fluorometric method, the A549 cells (2×10^6 cells/well) were seeded and incubated in a six-well plate for 24 h to allow cell attachment. The plate was then placed at 4 °C for 30 min.[53] After removing the culture medium, each well was supplemented with 2 mL of dosing medium containing 6.25 μM of free MB or colloidal MB and incubated at 37 °C. At each sampling time (0, 0.5, 1, 1.5, 2, and 4 h), the medium was completely removed, and cells were washed twice with 2 mL of cold PBS (4 °C). Cellular amount of MB was extracted by 200 μL of DMSO (30 min incubation) and determined by direct fluorometric measurement (excitation/emission = 610 nm/690 nm, gain = 73), based on a standard curve of MB.

The flow cytometric method was described as below. A549 or MDA-MB-231 cells were seeded in a 6 cm dish (1×10^6 cells/dish) and allowed to attach in a culture medium for 24 h. Before drug treatment, the culture dishes were placed at 4 °C for 30 min. Then, the medium was replaced with 2 mL of dosing medium containing free MB or colloidal MB (at MB concentrations of 3.13, 6.25, and 10 μM). At different times (0, 0.25, 0.5, 0.75, 1, 2, 3, 4, and 6 h), the dosing solution was removed, and cells washed twice with 2 mL of cold PBS followed by trypsinization (with 1 mL of 0.05% trypsin) and centrifugation (1000 rpm, 5 min) to collect cells. After removing the supernatant, cells were resuspended with 750 μL of PBS, to which 250 μL of 16% formaldehyde was added to fix the cells. After fixation (20 min), the cell pellets were collected by centrifugation (1000 rpm, 5 min) and resuspended in 1 mL of PBS and then stored at 4 °C. Flow cytometric analysis was conducted using a flow cytometer (Cytoflex, Beckman Coulter) with the following parameters: 638 nm laser; APC-700 filter; forward versus side scatter (FSC vs SSC) gating; 15,000 events.

AUTHOR INFORMATION

Corresponding Author

Teh-Min Hu − *Institute of Biopharmaceutical Sciences and Department of Pharmacy, National Yang Ming Chiao Tung University, Taipei 112, Taiwan;* orcid.org/0000-0001-6350-3180; Email: tehmin@nycu.edu.tw

Author

Guann-Tyng Chen − *Institute of Biopharmaceutical Sciences, National Yang Ming Chiao Tung University, Taipei 112, Taiwan; Tri-Service General Hospital, Beitou-Branch, Taipei 112, Taiwan*

Complete contact information is available at: https://pubs.acs.org/10.1021/acsomega.1c04877

Author Contributions

The manuscript was written through the contributions of all authors. All authors have given approval to the final version of the manuscript.

Notes

The authors declare no competing financial interest.

ACKNOWLEDGMENTS

The authors acknowledge the funding from the Ministry of Science and Technology, Taiwan (MOST 105-2320-B-016-006-MY3 and MOST 108-2320-B-010-037-MY3), the Higher Education Sprout Project of the National Yang Ming Chiao Tung University and Ministry of Education (MOE), Taiwan, and Tri-Service General Hospital, Beitou-Branch, Taipei, Taiwan (TSGH-BT_D_110007).

REFERENCES

(1) Ohlow, M. J.; Moosmann, B. Phenothiazine: the Seven Lives of Pharmacology's First Lead Structure. *Drug Discovery Today* **2011**, *16*, 119−131.

(2) Oz, M.; Lorke, D. E.; Hasan, M.; Petroianu, G. A. Cellular and Molecular Actions of Methylene Blue in the Nervous System. *Med. Res. Rev.* **2011**, *31*, 93−117.

(3) *Methylene Blue (injection)*. https://www.drugs.com/mtm/methylene-blue-injection.html (accessed Oct 27, 2021).

(4) Li, J.; Chen, X.; Qi, M.; Li, Y. Sentinel Lymph Node Biopsy Mapped with Methylene Blue Dye Alone in Patients with Breast Cancer: A Systematic Review and Meta-Analysis. *PLoS One* **2018**, *13*, e0204364−e0204364.

(5) Preiser, J.-C.; Lejeune, P.; Roman, A.; Carlier, E.; De Backer, D.; Leeman, M.; Kahn, R. J.; Vincent, J.-L. Methylene Blue Administration in Septic Shock: A Clinical Trial. *Crit. Care Med.* **1995**, *23*, 259−264.

(6) Küpfer, A.; Aeschlimann, C.; Cerny, T. Methylene Blue and the Neurotoxic Mechanisms of Ifosfamide Encephalopathy. *Eur. J. Clin. Pharmacol.* **1996**, *50*, 249−252.

(7) Pelgrims, J.; De Vos, F.; Van den Brande, J.; Schrijvers, D.; Prové, A.; Vermorken, J. B. Methylene blue in the Treatment and Prevention of Ifosfamide-Induced Encephalopathy: Report of 12 Cases and A Review of the Literature. *Br. J. Cancer* **2000**, *82*, 291−294.
(8) Schirmer, R. H.; Adler, H.; Pickhardt, M.; Mandelkow, E. Lest We Forget You — Methylene Blue ... *Neurobiol. Aging* **2011**, *32*, 2325.e7−2325.e16.
(9) Dabholkar, N.; Gorantla, S.; Dubey, S. K.; Alexander, A.; Taliyan, R.; Singhvi, G. Repurposing methylene blue in the management of COVID-19: mechanistic aspects and clinical investigations. *Biomed. Pharmacother.* **2021**, *142*, 112023.
(10) Tardivo, J. P.; Del Giglio, A.; de Oliveira, C. S.; Gabrielli, D. S.; Junqueira, H. C.; Tada, D. B.; Severino, D.; de Fátima Turchiello, R.; Baptista, M. S. Methylene blue in Photodynamic Therapy: From Basic Mechanisms to Clinical Applications. *Photodiagn. Photodyn. Ther.* **2005**, *2*, 175−191.
(11) König, K.; Bockhorn, V.; Dietel, W.; Schubert, H. Photochemotherapy of Animal Tumors with the Photosensitizer Methylene Blue Using A Krypton Laser. *J. Cancer Res. Clin. Oncol.* **1987**, *113*, 301−303.
(12) Junqueira, H. C.; Severino, D.; Dias, L. G.; Gugliotti, M. S.; Baptista, M. S. Modulation of Methylene Blue Photochemical Properties Based on Adsorption at Aqueous Micelle Interfaces. *Phys. Chem. Chem. Phys.* **2002**, *4*, 2320−2328.
(13) Wu, P.-T.; Lin, C.-L.; Lin, C.-W.; Chang, N.-C.; Tsai, W.-B.; Yu, J. Methylene-Blue-Encapsulated Liposomes as Photodynamic Therapy Nano Agents for Breast Cancer Cells. *Nanomaterials* **2019**, *9*, 14.
(14) Tang, W.; Xu, H.; Kopelman, R.; Philbert, M. A. Photodynamic Characterization and in Vitro Application of Methylene Blue-Containing Nanoparticle Platforms. *Photochem. Photobiol.* **2005**, *81*, 242−249.
(15) He, X.; Wu, X.; Wang, K.; Shi, B.; Hai, L. Methylene Blue-Encapsulated Phosphonate-Terminated Silica Nanoparticles for Simultaneous In vivo Imaging and Photodynamic Therapy. *Biomaterials* **2009**, *30*, 5601−5609.
(16) Wang, J.; Xu, D.; Deng, T.; Li, Y.; Xue, L.; Yan, T.; Huang, D.; Deng, D. Self-Decomposable Mesoporous Doxorubicin@Silica Nanocomposites for Nuclear Targeted Chemo-Photodynamic Combination Therapy. *ACS Appl. Nano Mater.* **2018**, *1*, 1976−1984.
(17) Ding, T. S.; Huang, X. C.; Luo, Y. L.; Hsu, H. Y. In Vitro Investigation of Methylene Blue-Bearing, Electrostatically Assembled Aptamer-Silica Nanocomposites as Potential Photodynamic Therapeutics. *Colloids Surf., B* **2015**, *135*, 217−224.
(18) Yan, F.; Zhang, Y.; Kim, K. S.; Yuan, H.-K.; Vo-Dinh, T. Cellular Uptake and Photodynamic Activity of Protein Nanocages Containing Methylene Blue Photosensitizing Drug. *Photochem. Photobiol.* **2010**, *86*, 662−666.
(19) Hah, H. J.; Kim, G.; Lee, Y.-E. K.; Orringer, D. A.; Sagher, O.; Philbert, M. A.; Kopelman, R. Methylene Blue-Conjugated Hydrogel Nanoparticles and Tumor-Cell Targeted Photodynamic Therapy. *Macromol. Biosci.* **2011**, *11*, 90−99.
(20) Lee, Y. D.; Cho, H. J.; Choi, M. H.; Park, H.; Bang, J.; Lee, S.; Kwon, I. C.; Kim, S. Directed Molecular Assembly into a Biocompatible Photosensitizing Nanocomplex for Locoregional Photodynamic Therapy. *J. Controlled Release* **2015**, *209*, 12−19.
(21) Seong, D.-Y.; Kim, Y.-J. Enhanced Photodynamic Therapy Efficacy of Methylene Blue-Loaded Calcium Phosphate Nanoparticles. *J. Photochem. Photobiol., B* **2015**, *146*, 34−43.
(22) Sahu, A.; Choi, W. I.; Lee, J. H.; Tae, G. Graphene Oxide Mediated Delivery of Methylene Blue for Combined Photodynamic and Photothermal Therapy. *Biomaterials* **2013**, *34*, 6239−6248.
(23) Hosseinzadeh, R.; Khorsandi, K.; Hosseinzadeh, G. Graphene Oxide-Methylene Blue Nanocomposite in Photodynamic Therapy of Human Breast Cancer. *J. Biomol. Struct. Dyn.* **2018**, *36*, 2216−2223.
(24) Seo, S.-H.; Kim, B.-M.; Joe, A.; Han, H.-W.; Chen, X.; Cheng, Z.; Jang, E.-S. NIR-Light-Induced Surface-Enhanced Raman Scattering for Detection and Photothermal/Photodynamic Therapy of Cancer Cells Using Methylene Blue-embedded Gold Nanorod@SiO2 Nanocomposites. *Biomaterials* **2014**, *35*, 3309−3318.
(25) Yu, J.; Hsu, C.-H.; Huang, C.-C.; Chang, P.-Y. Development of Therapeutic Au−Methylene Blue Nanoparticles for Targeted Photodynamic Therapy of Cervical Cancer Cells. *ACS Appl. Mater. Interfaces* **2015**, *7*, 432−441.
(26) Wang, H.; Bao, Y.; Qiu, H.; Tong, W. Encapsulation of Methylene Blue in Zeolitic Imidazolate Framework-90 Nanoparticles to Protect Its Photodynamic Activity. *Langmuir* **2020**, *36*, 6811−6818.
(27) Cheng, R.; Feng, F.; Meng, F.; Deng, C.; Feijen, J.; Zhong, Z. Glutathione-responsive nano-vehicles as a promising platform for targeted intracellular drug and gene delivery. *J. Controlled Release* **2011**, *152*, 2−12.
(28) El-Sawy, H. S.; Al-Abd, A. M.; Ahmed, T. A.; El-Say, K. M.; Torchilin, V. P. Stimuli-responsive nano-architecture drug-delivery systems to solid tumor micromilieu: past, present, and future perspectives. *ACS Nano* **2018**, *12*, 10636−10664.
(29) Croissant, J. G.; Fatieiev, Y.; Khashab, N. M. Degradability and Clearance of Silicon, Organosilica, Silsesquioxane, Silica Mixed Oxide, and Mesoporous Silica Nanoparticles. *Adv. Mater.* **2017**, *29*, 1604634.
(30) Du, X.; Kleitz, F.; Li, X.; Huang, H.; Zhang, X.; Qiao, S.-Z. Disulfide-Bridged Organosilica Frameworks: Designed, Synthesis, Redox-Triggered Biodegradation, and Nanobiomedical Applications. *Adv. Funct. Mater.* **2018**, *28*, 1707325.
(31) Quignard, S.; Masse, S.; Laurent, G.; Coradin, T. Introduction of Disulfide Bridges within Silica Nanoparticles to Control their Intra-Cellular Degradation. *Chem. Commun.* **2013**, *49*, 3410−3412.
(32) Hayashi, K.; Maruhashi, T.; Nakamura, M.; Sakamoto, W.; Yogo, T. One-Pot Synthesis of Dual Stimulus-Responsive Degradable Hollow Hybrid Nanoparticles for Image-Guided Trimodal Therapy. *Adv. Funct. Mater.* **2016**, *26*, 8613−8622.
(33) Huang, X.-C.; Wu, L.-B.; Hsu, J.-F.; Shigeto, S.; Hsu, H.-Y. Biothiol-Triggered, Self-Disassembled Silica Nanobeads for Intracellular Drug Delivery. *Acta Biomater.* **2015**, *23*, 263−270.
(34) Croissant, J.; Cattoën, X.; Man, M. W. C.; Gallud, A.; Raehm, L.; Trens, P.; Maynadier, M.; Durand, J.-O. Biodegradable Ethylene-Bis(Propyl)Disulfide-Based Periodic Mesoporous Organosilica Nanorods and Nanospheres for Efficient in Vitro Drug Delivery. *Adv. Mater.* **2014**, *26*, 6174−6180.
(35) Zhou, M.; Du, X.; Li, W.; Li, X.; Huang, H.; Liao, Q.; Shi, B.; Zhang, X.; Zhang, M. One-pot Synthesis of Redox-Triggered Biodegradable Hybrid Nanocapsules with A Disulfide-Bridged Silsesquioxane Framework for Promising Drug Delivery. *J. Mater. Chem. B* **2017**, *5*, 4455−4469.
(36) Wu, M.; Chen, W.; Chen, Y.; Zhang, H.; Liu, C.; Deng, Z.; Sheng, Z.; Chen, J.; Liu, X.; Yan, F.; Zheng, H. Focused Ultrasound-Augmented Delivery of Biodegradable Multifunctional Nanoplatforms for Imaging-Guided Brain Tumor Treatment. *Adv. Sci.* **2018**, *5*, 1700474.
(37) Chen, Y.; Meng, Q.; Wu, M.; Wang, S.; Xu, P.; Chen, H.; Li, Y.; Zhang, L.; Wang, L.; Shi, J. Hollow Mesoporous Organosilica Nanoparticles: A Generic Intelligent Framework-Hybridization Approach for Biomedicine. *J. Am. Chem. Soc.* **2014**, *136*, 16326−16334.
(38) Hadipour Moghaddam, S. P.; Saikia, J.; Yazdimamaghani, M.; Ghandehari, H. Redox-Responsive Polysulfide-Based Biodegradable Organosilica Nanoparticles for Delivery of Bioactive Agents. *ACS Appl. Mater. Interfaces* **2017**, *9*, 21133−21146.
(39) Yu, L.; Chen, Y.; Lin, H.; Du, W.; Chen, H.; Shi, J. Ultrasmall Mesoporous Organosilica Nanoparticles: Morphology Modulations and Redox-Responsive Biodegradability for Tumor-Specific Drug Delivery. *Biomaterials* **2018**, *161*, 292−305.
(40) Quesada, M.; Muniesa, C.; Botella, P. Hybrid PLGA-Organosilica Nanoparticles with Redox-Sensitive Molecular Gates. *Chem. Mater.* **2013**, *25*, 2597−2602.
(41) Maggini, L.; Cabrera, I.; Ruiz-Carretero, A.; Prasetyanto, E. A.; Robinet, E.; De Cola, L. Breakable Mesoporous Silica Nanoparticles for Targeted Drug Delivery. *Nanoscale* **2016**, *8*, 7240−7247.

https://doi.org/10.1021/acsomega.1c04877
ACS Omega 2021, 6, 32109−32119

(42) Yang, Y.; Wan, J.; Niu, Y.; Gu, Z.; Zhang, J.; Yu, M.; Yu, C. Structure-Dependent and Glutathione-Responsive Biodegradable Dendritic Mesoporous Organosilica Nanoparticles for Safe Protein Delivery. *Chem. Mater.* **2016**, *28*, 9008−9016.
(43) Chou, H.-C.; Chiu, S.-J.; Liu, Y.-L.; Hu, T.-M. Direct formation of S-nitroso silica nanoparticles from a single silica source. *Langmuir* **2014**, *30*, 812−822.
(44) Chiu, S.-J.; Wang, S.-Y.; Chou, H.-C.; Liu, Y.-L.; Hu, T.-M. Versatile synthesis of thiol-and amine-bifunctionalized silica nanoparticles based on the ouzo effect. *Langmuir* **2014**, *30*, 7676−7686.
(45) Kim, J. H.; Fang, B.; Song, M. Y.; Yu, J.-S. Topological Transformation of Thioether-Bridged Organosilicas into Nanostructured Functional Materials. *Chem. Mater.* **2012**, *24*, 2256−2264.
(46) Wang, M.-R.; Chiu, S.-J.; Chou, H.-C.; Hu, T.-M. An efficient S-NO-polysilsesquioxane nano-platform for the co-delivery of nitric oxide and an anticancer drug. *Chem. Commun.* **2015**, *51*, 15649−15652.
(47) Chiu, S.-J.; Lin, C.-Y.; Chou, H.-C.; Hu, T.-M. Silica ouzo effect: amphiphilic drugs facilitate nanoprecipitation of polycondensed mercaptosilanes. *Langmuir* **2016**, *32*, 211−220.
(48) Lin, S.-Y.; Wang, M.-R.; Chiu, S.-J.; Lin, C.-Y.; Hu, T.-M. S-Nitrosothiols (SNO) as light-responsive molecular activators for post-synthesis fluorescence augmentation in fluorophore-loaded nanospheres. *J. Mater. Chem. B* **2018**, *6*, 153−164.
(49) Su, Y.-L.; Lin, C.-Y.; Chiu, S.-J.; Hu, T.-M. Formation of organosilica nanoparticles with dual functional groups and simultaneous payload entrapment. *J. Microencapsulation* **2018**, *35*, 381−391.
(50) White, V. R.; Fitzgerald, J. M. Continuous determination ascorbic acid by photobleaching of methylene blue. *Anal. Chem.* **1972**, *44*, 1267−1269.
(51) Wilhelm, S.; Tavares, A. J.; Dai, Q.; Ohta, S.; Audet, J.; Dvorak, H. F.; Chan, W. C. Analysis of nanoparticle delivery to tumours. *Nat. Rev. Mater.* **2016**, *1*, 1−12.
(52) Chittasupho, C.; Lirdprapamongkol, K.; Kewsuwan, P.; Sarisuta, N. Targeted delivery of doxorubicin to A549 lung cancer cells by CXCR4 antagonist conjugated PLGA nanoparticles. *Eur. J. Pharm. Biopharm.* **2014**, *88*, 529−538.
(53) Lesniak, A.; Salvati, A.; Santos-Martinez, M. J.; Radomski, M. W.; Dawson, K. A.; Åberg, C. Nanoparticle adhesion to the cell membrane and its effect on nanoparticle uptake efficiency. *J. Am. Chem. Soc.* **2013**, *135*, 1438−1444.

https://doi.org/10.1021/acsomega.1c04877
ACS Omega 2021, 6, 32109−32119